Physical vs phantom dark energy after DESI: thawing quintessence in a curved background

Bikash R. Dinda [1,2,*] and Roy Maartens [1,2,†]

[1] *Department of Physics & Astronomy, University of the Western Cape, Cape Town 7535, South Africa.*

[2] *National Institute for Theoretical & Computational Science, Cape Town 7535, South Africa*

Recent data from DESI, in combination with other data, provide moderate evidence of dynamical dark energy, $w \neq -1$. In the w_0, w_a parametrization of w, there is a preference for a phantom crossing, $w < -1$, at redshift $z \sim 0.5$. In general relativity, the phantom equation of state is unphysical. Thus it is important to check whether phantom crossing is present in other physically self-consistent models of dark energy that have equivalent evidence to the w_0, w_a parametrization. We find that thawing quintessence with nonzero cosmic curvature can fit the recent data slightly better than w_0, w_a in a flat background. The phantom crossing may be a spurious artifact of a parametrization that is not based on a physical model.

PACS numbers:

The Dark Energy Spectroscopic Instrument (DESI) Data Releases DR1 and DR2 [1–5] have delivered state-of-the-art precision on baryon acoustic oscillation (BAO) measurements. This has facilitated stringent constraints on the dark energy equation of state, w. Using the parametrization

$$w(z) = w_0 + w_a \frac{z}{1+z}\,, \tag{1}$$

both DESI DR1 and DR2 BAO favour a phantom crossing, from a phantom value $w < -1$ at earlier times, $z \gtrsim 0.5$, to $w > -1$ for $z \lesssim 0.5$. Phantom behavior is unphysical in general relativity since energy conservation implies the growth of dark energy density with expansion, $\dot{\rho}_{\rm de} > 0$. It is implied by similar parametrizations which are not based on physical models of w (e.g., see Fig. 4 in [5]). For a physically motivated model, DESI data suggest that we consider dark energy models which behave close to a cosmological constant $w = -1$ at early times, with an increase to $w > -1$ at late times (e.g., see Figs. 11 and 12 in [5]). Physically consistent examples are provided by the 'thawing' class of quintessence models [6, 7].

To investigate the robustness of this phantom crossing, we start by showing the DESI DR2 BAO data for $\tilde{D}_M = D_M/r_d$ and $\tilde{D}_H = D_H/r_d$ (where D_M and D_H are comoving and Hubble distances and r_d is the comoving sound horizon at baryon drag). We also show the best fit ΛCDM in the flat (Figure 1) and negatively curved oΛCDM (Figure 2) cases, using also the CMB distance prior, as in DESI DR2 [4] (see their Appendix A). From Figure 1 and Figure 2 it is clear that at earlier times ($z \gtrsim 1.5$) the deviations from both ΛCDM and oΛCDM model are well within 1σ. At intermediate times

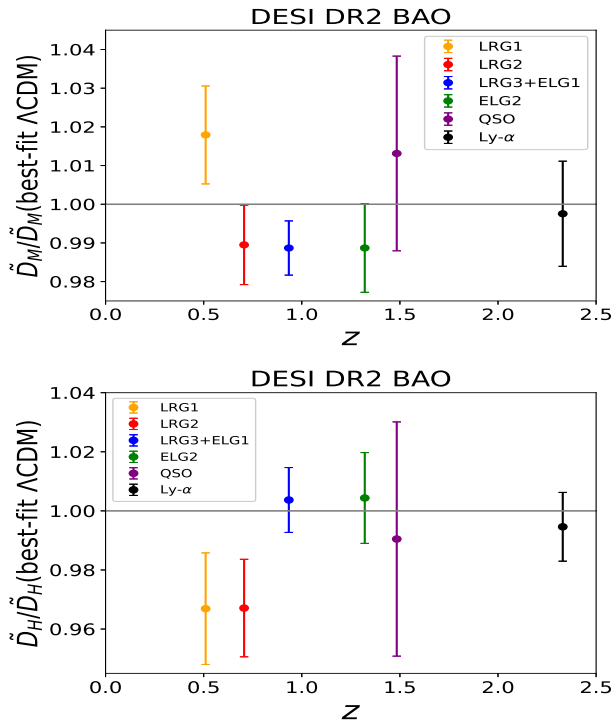

FIG. 1: Comparison of $\tilde{D}_M = D_M/r_d$ (upper panel) and $\tilde{D}_H = D_H/r_d$ (lower panel) to the best-fit values of flat ΛCDM, obtained from CMB+DESI DR2 BAO.

($0.9 \gtrsim z \gtrsim 1.5$) the deviations are $\sim 1\sigma$, and at late times $z \lesssim 0.9$ the deviations are $\lesssim 2\sigma$. Note that these results are similar to the lower panels of Fig. 6 in [4]. These plots hint that there is no evidence for deviation from ΛCDM (or oΛCDM) at higher redshifts ($z \gtrsim 1.5$). At intermediate redshifts ($0.9 \gtrsim z \gtrsim 1.5$) there is no significant deviation either. This is evidence that the phantom

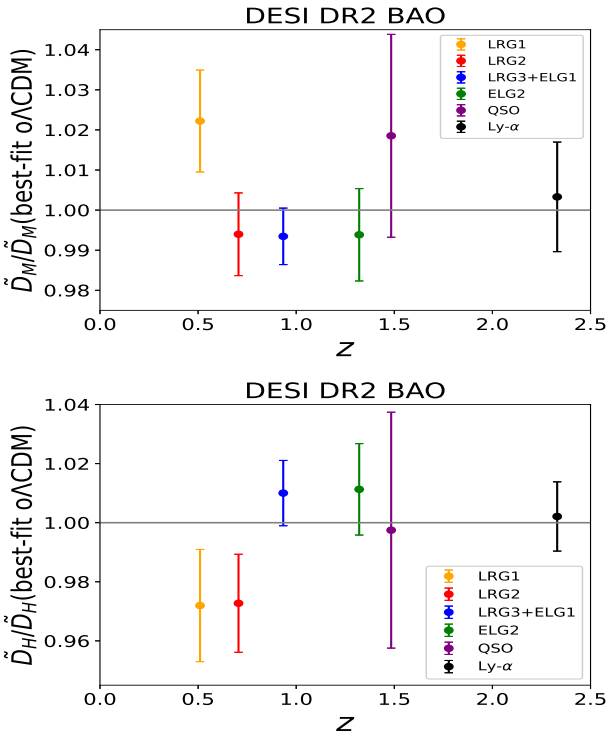

FIG. 2: As in Figure 1 but for best-fit oΛCDM values.

crossing is a model-dependent artifact of the w_0w_aCDM model. Evidently, the w_0w_aCDM or similar parametrizations are too simplistic to correctly capture the behavior at lower and higher redshifts simultaneously.

Figure 1 and Figure 2 also reveal another interesting feature. In flat ΛCDM, $\tilde{D}_H = \tilde{D}'_M$ so that the deviations in $\tilde{D}_M$ and $\tilde{D}_H$ should be similar in the flat case.However, DESI DR2 data shows that the deviations are different in $\tilde{D}_M$ and $\tilde{D}_H$ at intermediate redshifts. The DESI DR2 main paper [4] finds the constraint $10^3\Omega_{K0} = 2.3 \pm 1.1$ on cosmic curvature (their Table V). Of course, inferences about curvature may not hold for dynamical dark energy, since in that case, w is partially degenerate with Ω_{K0}.

At this stage, our task is half complete, because the intermediate to higher redshift behavior can be well modeled by the oΛCDM model, but definitely not the lower redshift results. The lower redshift data is what allows w_0w_aCDM or similar parametrizations to show a hint of deviations from ΛCDM and of phantom crossing even in the presence of nonzero cosmic curvature. The oΛCDM model cannot properly capture the behavior over the entire redshift range either. Consequently, our next step is to find a physically consistent model which can capture the behavior for the whole redshift

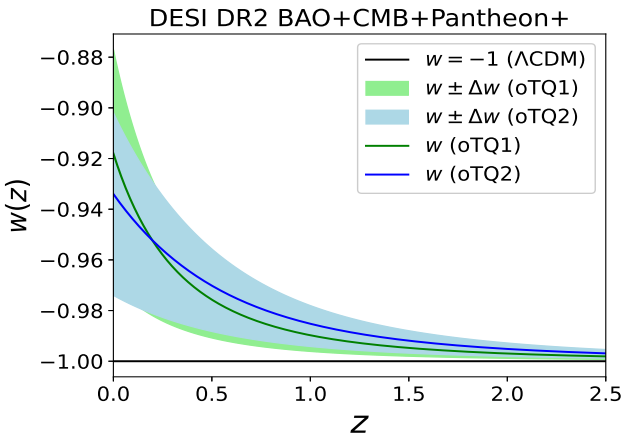

FIG. 3: Thawing quintessence models oTQ1,2. Constraints on w_0 are from DESI DR2 BAO + CMB + Pantheon+.

range.

We consider quintessence dark energy models, which have self-consistent physical properties, including $w \geq -1$ and a speed of sound $c_s = 1$ [8–10]. Quintessence models cover a huge range of behavior, but we focus on the thawing class (TQ) which naturally produces $w > -1$ at low redshift, as suggested by the predictions in w_0w_aCDM and similar parametrizations (see Fig. 4 [5]). We also include cosmic curvature (oTQ). For generality, we use two parametrisations of w which approximate thawing quintessence models, as shown in [6, 7, 11]:

$$w(z) = -1 + \frac{1+w_0}{(1+z)^3}, \quad (2)$$

$$w(z) = -1 + \frac{3^{2/3}(1+w_0)\left(z^3+3z^2+3z+3\right)^{-2/3}}{1+z}. \quad (3)$$

We identify these 1-parameter w models as oTQ1 and oTQ2. The Hubble rate is given by

$$\frac{H^2}{H_0^2} = \Omega_{r0}(1+z)^4 + \Omega_{m0}(1+z)^3 + \Omega_{K0}(1+z)^2 + \Omega_{q0}\exp\left[3\int_0^z \frac{1+w(\tilde{z})}{1+\tilde{z}}d\tilde{z}\right], \quad (4)$$

where $\Omega_{r0} + \Omega_{m0} + \Omega_{K0} + \Omega_{q0} = 1$.

Figure 3 shows the mean $w(z)$ for oTQ1,2 as given by Equation 2, Equation 3, with 1σ shaded regions. Constraints are from DESI DR2 BAO+CMB+Pantheon+. The quintessence models do not allow $w_0 < -1$, but this is not automatically enforced in the $w(z)$ parametrizations. If we impose a prior $w_0 < -1$ in the data analysis, it does not alter the results in Figure 3. This shows that there is no evidence of phantom crossing in these models.

In order to make a stronger statement, we should show that the oTQ models are at the same (or better) evidence level as w_0w_aCDM. To this end, we compare the best-fit log-likelihood values of these models:

$$\ln L\,(\text{oTQ1,2}) - \ln L(w_0w_a\text{CDM}) = (0.47,\ 0.37)\,. \quad (5)$$

Since the number of parameters is the same in all three models, the best-fit log-likelihood comparison is enough to show the model comparison. We see that oTQ1 and oTQ2 are slightly preferred over w_0w_aCDM. Although this is not significant, it is enough to show that the phantom crossing is not inevitable or even preferred.

A dark energy parametrization is a simple and useful way to do data analysis in cosmology – but preferably we need to show that a physically motivated model of dark energy, in this case a realistic thawing quintessence, produces similar results [3, 12–22]. We consider a class of realistic thawing quintessence models in the presence of cosmic curvature. In the presence of matter, radiation, and curvature, a general quintessence field obeys the evolution equations [23–26]:

$$\begin{aligned}
\frac{\mathrm{d}w}{\mathrm{d}N} &= (w-1)\Big(3w+3-\lambda\sqrt{3(w+1)\Omega_\mathrm{q}}\Big),\\
\frac{\mathrm{d}\Omega_\mathrm{q}}{\mathrm{d}N} &= \Omega_\mathrm{q}\big[3w\Omega_\mathrm{q}-3w-\Omega_\mathrm{K}+\Omega_\mathrm{r}\big],\\
\frac{\mathrm{d}\lambda}{\mathrm{d}N} &= -\sqrt{3}(\Gamma-1)\lambda^2\sqrt{(w+1)\Omega_\mathrm{q}}\,,\\
\frac{\mathrm{d}\Omega_\mathrm{r}}{\mathrm{d}N} &= \Omega_\mathrm{r}\big[3w\Omega_\mathrm{q}-\Omega_\mathrm{K}+\Omega_\mathrm{r}-1\big],\\
\frac{\mathrm{d}\Omega_\mathrm{K}}{\mathrm{d}N} &= \Omega_\mathrm{K}\big[3w\Omega_\mathrm{q}-\Omega_\mathrm{K}+\Omega_\mathrm{r}+1\big], \qquad (6)
\end{aligned}$$

where $N=\ln a$, the slope of the quintessence potential is $\lambda=-M_\mathrm{pl}V_\phi/V$ and $\Gamma=VV_{\phi\phi}/V_\phi^2$ (subscript ϕ denotes $\partial/\partial\phi$). For non-constant Γ and which cannot be explicitly expressed in terms of λ, one needs further differential equations that depend on the nature of the potential. We restrict our analysis to constant Γ, which includes exponential ($\Gamma=1$) and mononomial ($\Gamma=1+1/n$ for $V(\phi)=V_0\phi^{-n}$) potentials.

For thawing quintessence, initial values should be $0<w_\mathrm{i}+1\ll 1$ and $\lambda_\mathrm{i}>0$ [9, 23, 27–29]. We use $w_\mathrm{i}=10^{-4}-1$ and $\Gamma=5$ ($n=1/4$). We name this model oTQR (curved thawing quintessence realistic).

Using the best-fit cosmological density parameters from DESI DR2 BAO+CMB+Pantheon+ data, we can solve the system in Equation 6. The resulting $w(z)$ and $\Omega_\mathrm{q}(z)$ are shown in Figure 4. Figure 5 shows constraints on the model parameters through triangle plots.

As pointed out in [5], in order to find proper constraints on realistic quintessence parameters, we need to have data-informed priors on these parameters. However, this is true only for the energy density parameters Ω_qi, Ω_ri, and Ω_Ki, not for the other parameters. This is due to the cosmic coincidence problem, present in all realistic physical models [30–32]. If we try to mimic w_0w_aCDM by a physically motivated model, we will encounter the same coincidence problem. Thus this fact cannot be a negative point for model comparison.

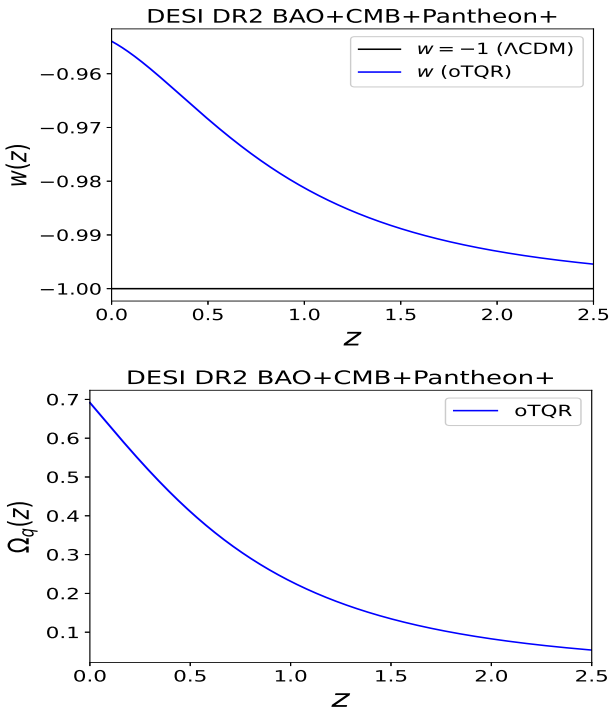

FIG. 4: $w(z)$ (upper panel) and $\Omega_\mathrm{q}(z)$ (lower panel) for a realistic thawing quintessence model (oTQR) with best-fit values obtained from DESI DR2 BAO+CMB+Pantheon+.

It is also argued in [5] that for realistic quintessence models to fit the data well, they must have a rapid increase of w for $z\lesssim 0.3$. However, the upper panel of Figure 4 shows that this statement is not applicable. Furthermore, it is argued that there might be features of a sharp increase in the energy density of dark energy – but the lower panel of Figure 4 shows no sharp increase.

Finally, we compare the best-fit log-likelihood of the realistic open thawing quintessence model oTQR to that of w_0w_aCDM:

$$\ln L\,(\text{oTQR}) - \ln L(w_0w_a\text{CDM}) = -0.03\,. \quad (7)$$

This shows that the evidence for curved realistic quintessence is effectively equivalent to that of flat w_0w_aCDM. We conclude that curved thawing quintessence is equivalently favored compared to

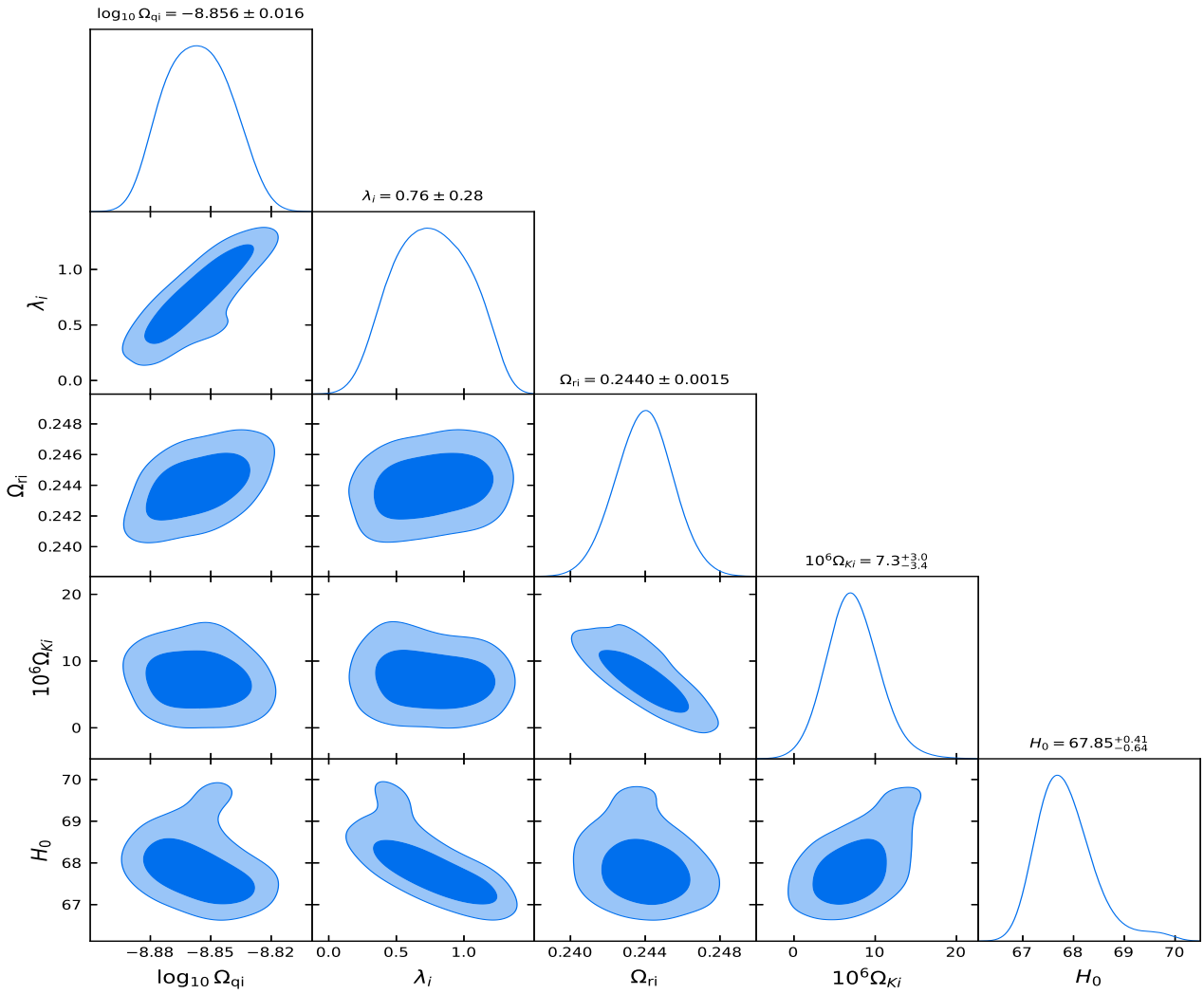

FIG. 5: Constraints on the oTQR model parameters for DESI DR2 BAO+CMB+Pantheon+ data.

w_0w_aCDM in light of DESI DR2 BAO data (in combination with other relevant observations). The evidence for phantom crossing is model-dependent.

Acknowledgments: We are supported by the South African Radio Astronomy Observatory and the National Research Foundation (Grant No. 75415).

* Electronic address: bikashrdinda@gmail.com
† Electronic address: roy.maartens@gmail.com

[1] A. G. Adame *et al.* (DESI), JCAP **02**, 021 (2025), arXiv:2404.03002 .
[2] R. Calderon *et al.* (DESI), JCAP **10**, 048 (2024), arXiv:2405.04216 .
[3] K. Lodha *et al.* (DESI), Phys. Rev. D **111**, 023532 (2025), arXiv:2405.13588 .
[4] M. Abdul Karim *et al.* (DESI), (2025), arXiv:2503.14738 .
[5] K. Lodha *et al.*, (2025), arXiv:2503.14743 .
[6] E. V. Linder, Gen. Rel. Grav. **40**, 329 (2008), arXiv:0704.2064 .
[7] E. V. Linder, Phys. Rev. D **91**, 063006 (2015), arXiv:1501.01634 .
[8] R. R. Caldwell and E. V. Linder, Phys. Rev. Lett. **95**, 141301 (2005), arXiv:astro-ph/0505494 .
[9] S. Tsujikawa, Class. Quant. Grav. **30**, 214003 (2013), arXiv:1304.1961 [gr-qc] .
[10] R. R. Caldwell, R. Dave, and P. J. Steinhardt, Phys. Rev. Lett. **80**, 1582 (1998), arXiv:astro-ph/9708069 .
[11] D. Shlivko, P. J. Steinhardt, and C. L. Steinhardt, (2025), arXiv:2504.02028 .
[12] Y. Akrami, G. Alestas, and S. Nesseris, (2025),

arXiv:2504.04226 .
[13] G. Borghetto, A. Malhotra, G. Tasinato, and I. Zavala, (2025), arXiv:2503.11628 .
[14] A. J. Shajib and J. A. Frieman, (2025), arXiv:2502.06929 .
[15] W. J. Wolf, C. García-García, and P. G. Ferreira, (2025), arXiv:2502.04929 .
[16] S. Dubey, S. Agrawal, A. Beesham, D. Sofuoğlu, and B. K. Shukla, Eur. Phys. J. Plus **140**, 254 (2025).
[17] Y. Tada and T. Terada, Phys. Rev. D **109**, L121305 (2024), arXiv:2404.05722 .
[18] O. F. Ramadan, J. Sakstein, and D. Rubin, Phys. Rev. D **110**, L041303 (2024), arXiv:2405.18747 .
[19] W. J. Wolf, C. García-García, D. J. Bartlett, and P. G. Ferreira, Phys. Rev. D **110**, 083528 (2024), arXiv:2408.17318 .
[20] M. Berbig, JCAP **03**, 015 (2025), arXiv:2412.07418 .
[21] S. Goldstein, M. Park, M. Raveri, B. Jain, and L. Samushia, Phys. Rev. D **107**, 063530 (2023), arXiv:2207.01612 .
[22] G. Payeur, E. McDonough, and R. Brandenberger, (2024), arXiv:2411.13637 .
[23] T. G. Clemson and A. R. Liddle, Mon. Not. Roy. Astron. Soc. **395**, 1585 (2009), arXiv:0811.4676 .
[24] B. R. Dinda, JCAP **09**, 035 (2017), arXiv:1705.00657 .
[25] S. Bhattacharya, G. Borghetto, A. Malhotra, S. Parameswaran, G. Tasinato, and I. Zavala, JCAP **09**, 073 (2024), arXiv:2405.17396 .
[26] D. Andriot, S. Parameswaran, D. Tsimpis, T. Wrase, and I. Zavala, JHEP **08**, 117 (2024), arXiv:2405.09323 .
[27] R. J. Scherrer and A. A. Sen, Phys. Rev. D **77**, 083515 (2008), arXiv:0712.3450 .
[28] T. Chiba, A. De Felice, and S. Tsujikawa, Phys. Rev. D **87**, 083505 (2013), arXiv:1210.3859 .
[29] B. R. Dinda and A. A. Sen, Phys. Rev. D **97**, 083506 (2018), arXiv:1607.05123 .
[30] I. Zlatev, L.-M. Wang, and P. J. Steinhardt, Phys. Rev. Lett. **82**, 896 (1999), arXiv:astro-ph/9807002 .
[31] V. Sahni and A. A. Starobinsky, Int. J. Mod. Phys. D **9**, 373 (2000), arXiv:astro-ph/9904398 .
[32] H. E. S. Velten, R. F. vom Marttens, and W. Zimdahl, Eur. Phys. J. C **74**, 3160 (2014), arXiv:1410.2509 .